

Application of the Diamond Gate in Quantum Fourier Transformations and Quantum Machine Learning

E. Bahnsen,¹ S. E. Rasmussen,¹ N. J. S. Loft,¹ and N. T. Zinner^{1,2,*}

¹*Department of Physics and Astronomy, Aarhus University, DK-8000 Aarhus C, Denmark*

²*Aarhus Institute of Advanced Studies, Aarhus University, DK-8000 Aarhus C, Denmark*

(Dated: May 16, 2022)

As we are approaching actual application of quantum technology it is important to exploit the current quantum resources the best possible way. With this in mind it might not be beneficial to use the usual standard gate sets, inspired from classical logic gates, when compiling quantum algorithms, when other less standardized gates currently perform better. We therefore consider a native gate, which occurs naturally in superconducting circuits, known as the diamond gate. We show how the diamond gate can be decomposed into standard gates and with the use of single-qubit gates can work as a controlled-not-swap (CNS) gate. We then show how this CNS gate can be used to create a controlled phase gate. Controlled phase gates are the backbone of the quantum Fourier transform algorithm and we therefore show how to use the diamond gate to perform this algorithm. We also show how to use the diamond gate in quantum machine learning, namely we use it to approximate non-linear functions and classify two-dimensional data.

INTRODUCTION

Quantum technology has acquired an increasing amount of attention in the last couple of years, especially since the quantum supremacy experiment at Google [1]. The search for quantum advantages in practical applications is an increasingly active area of research [2], and there is growing consensus that useful applications will be found in the Noisy Intermediate-Scale Quantum (NISQ) era [3]. In this era quantum technology supports only a couple of tens of qubits and a few hundred gate operations before the noise becomes too overwhelming.

In this era we must work with the native gates of quantum systems, despite their imperfections compared to the set of standard gates, composed of gates such as the CNOT or Fredkin gate. An example of such a native gate is the diamond gate [4], which has the advantage of being a naturally arising highly entangling four-qubit gate in superconducting circuits. However, it has the disadvantage of being a complex gate to understand and thus use in quantum algorithm circuits. In this paper we seek to demystify the gate and show its various applications in synthesizing other quantum gates, performing quantum algorithms, and taking part in quantum machine learning. The aim of this paper is to show the utility of the diamond gate, as well as showing a different approach to quantum circuitry using some currently available gates rather than some of the more inaccessible standard gates.

The diamond gate is closely related to the Fredkin gate, which is often used in a set of standard gates for quantum computation [5]. In particular, they are both controlled swapping gates, however, the diamond has a pair of control qubits, which must be in a Bell-state for the closed state of the gate. Other implementations of controlled swapping gates besides the Fredkin gate [6–14]

includes superconducting qubits in a waveguide cavity [15], linear superconducting qubits [16], and multi-controlled *i*SWAP gates [17].

A popular approach to optimize the computational power is to divide the computational task between classical and quantum resources, i.e. a so-called hybrid quantum classical (HQC) algorithm. Examples of such HQC algorithms are the quantum approximate optimization algorithm (QAOA) [18–20], quantum autoencoder (QAE) [21], quantum variational error corrector (QVECTOR) [22], classification via near term quantum neural network (QNN) [23–26], quantum generative adversarial network (qGAN) [27–30], and variational quantum eigensolver (VQE) [31–38].

Common for all these HQC algorithms is that they share a subroutine for producing parameterized trial states, where the parameters can be tuned to optimize a function value. The performance of these algorithms depends on the configuration of the parameterized quantum circuit (PQC) [39–42]. Many of the HQC algorithms draw inspiration from classical machine learning algorithms. Therefore PQCs are often considered the quantum mechanical equivalent to neural networks, which is why they are sometimes referred to as quantum neural networks [23–26]. In this paper we apply the diamond gate to quantum circuit learning [43] and classification via QNNs [26] using the diamond gate as an entangling gate in a PQC. Previously the diamond gate has been used in VQE algorithms [44]. Besides HQC algorithms we also consider the diamond gate for performing quantum Fourier transformations (QFT), which are used to estimate the phase of quantum mechanical amplitudes. This could be used to solve the order-finding problem or the factoring problem [5].

In this paper we show how the diamond gate can be operated as a native controlled-phase gate. We then use this to perform the quantum Fourier transform with the diamond gate. We also apply the diamond gate to machine learning problems. In particular, we apply it to a

* zinner@phys.au.dk

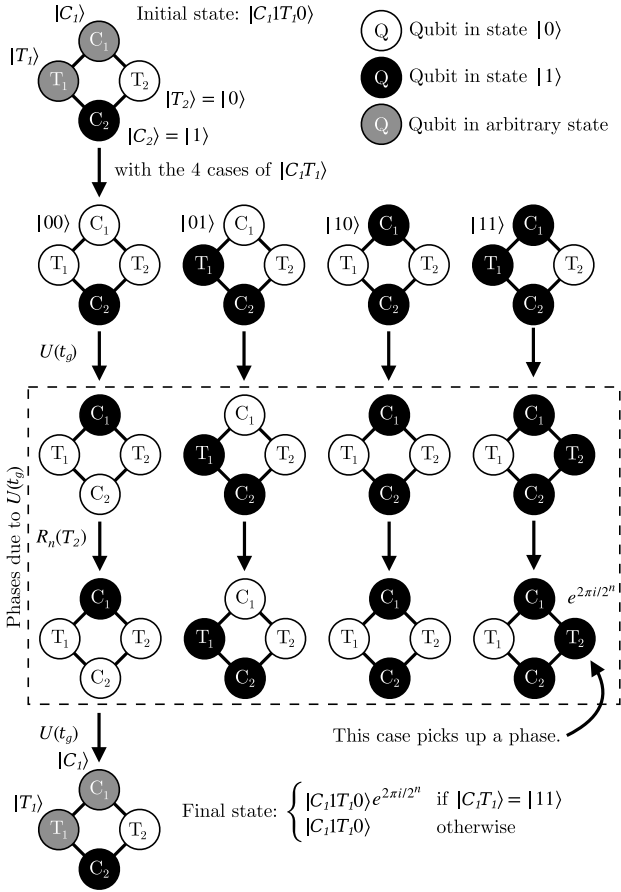


Figure 1. **Flow chart of native diamond gate implementing a controlled R_n -gate**. The qubits start in the state $|C_1T_1,0\rangle$, and will by the end pick up a phase $e^{2\pi i/2^n}$ if and only if both control and target qubit are in the $|1\rangle$ -state. The flow chart corresponds to the circuit diagram in Eq. (3).

problem of quantum circuit learning [43] and classification of two-dimensional data [26]. The methods used in order to use the diamond gate for these applications are based on a decomposition of the gate and are shown in the Methods section

RESULTS

Native gate derivatives

The diamond gate [4] can be worked as a controlled SWAP or phase gate (See Methods section). This is particularly useful in the construction of a QFT-circuit which is highly dependent on controlled phase gates, in particular QFT is dependent on the implementation of the controlled R_n -gate (see Fig. 2)

$$R_n = R_z(2\pi/2^n) = \begin{pmatrix} 1 & 0 \\ 0 & e^{2\pi i/2^n} \end{pmatrix}. \quad (1)$$

Such a gate can be implemented following the prescription in Ref. [45], which derive different ways of decomposing the controlled R_n -gate, but we use the approach with one auxiliary qubit, such that three of the four diamond-qubits are in use like so:

$$|0\rangle \text{---} \boxed{R_n} \text{---} |0\rangle = |0\rangle \text{---} \begin{matrix} \text{---} \times \text{---} \\ \text{---} \times \text{---} \end{matrix} \boxed{R_n} \begin{matrix} \text{---} \times \text{---} \\ \text{---} \times \text{---} \end{matrix} |0\rangle \quad (2)$$

which locks one of the qubits in the $|0\rangle$ state. Our approach is to use the diamond instead of the controlled SWAP gates. This introduces one extra qubit, and due to the symmetry of the diamond we can pick this to be any of the four diamond qubits. We chose C_2 for this task and fix it in a $|1\rangle$ state. We then pick the other control qubit, C_1 , as the control of the R_n -gate above, while we choose T_1 as the target, and finally T_2 will be the ancillary qubit in the $|0\rangle$ state. The circuit diagram takes the form

$$\begin{matrix} |C_1\rangle \\ |1\rangle \\ |T_1\rangle \\ |0\rangle \end{matrix} \text{---} \boxed{R_n} \text{---} \begin{matrix} |C_1\rangle \\ |1\rangle \\ |T_1\rangle \\ |0\rangle \end{matrix} = \begin{matrix} |C_1\rangle \\ |1\rangle \\ |T_1\rangle \\ |0\rangle \end{matrix} \text{---} U(t_g) \text{---} \begin{matrix} \text{---} \times \text{---} \\ \text{---} \times \text{---} \end{matrix} \boxed{R_n} \begin{matrix} \text{---} \times \text{---} \\ \text{---} \times \text{---} \end{matrix} U(t_g) \text{---} \begin{matrix} |C_1\rangle \\ |1\rangle \\ |T_1\rangle \\ |0\rangle \end{matrix} \quad (3)$$

In order to understand this circuit diagram properly we consider the four different possibilities for two undetermined qubits C_1 and T_1 , i.e., we consider the four different possibilities for the state $|C_1T_1\rangle$. Note that the four possibilities we consider is a complete basis for the two qubits. We want the qubit to obtain an overall factor $e^{2\pi i/2^n}$ only when $|C_1T_1\rangle = |11\rangle$. The four different cases are presented in Fig. 1 from which we see that the phase is only obtained in the desired case.

We start with the one control and one target qubit in the state $|C_2T_2\rangle = |10\rangle$, while the two other qubits are in a arbitrary state $|C_1T_1\rangle$. In Fig. 1 we branch out to the four different possibilities $|0100\rangle$, $|0110\rangle$, $|1100\rangle$, and $|1110\rangle$. When we apply the first $U(t_g)$ gate we effectively compare the states of control qubits C_1 and C_2 and if they are equal the states of T_1 and T_2 are swapped. This happens in the fourth branch of Fig. 1. In the third branch, the states of the target qubits are the same, and thus no swapping occurs. Due to the symmetry of the diamond gate the states of the target qubits are also compared, and the control qubit states are swapped accordingly. This is what happens in the first branch. In the second branch, the target qubit states are different and no control state is swapped. When we apply the $R_n^{T_2}$ gate only the fourth branch picks up the phase, as it is the only case for which T_2 is in the $|1\rangle$ state. Finally, when we apply the $U(t_g)$ gate again we swap the states back, and the qubits have obtained an overall phase if and only if the original state was $|1110\rangle$.

Phase programming

As mentioned in the beginning of the section the diamond gate is symmetric in the target and control qubits.

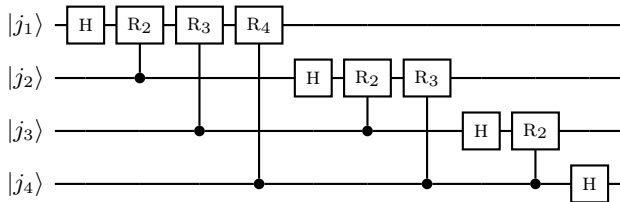
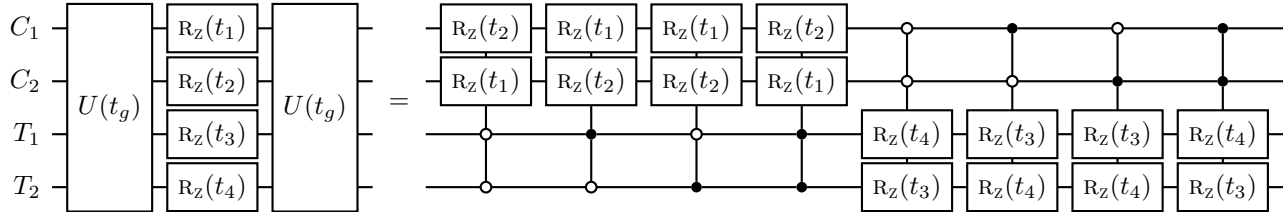


Figure 2. **Quantum Fourier transform circuit with four qubits** A single Hadamard gate and multiple controlled phase gates are applied to each qubit in order to perform QFT [5].

This allows us to program what controlled phase gates to keep, by fixing the states of some of the qubits, as well as choosing different values of t_i . If we set $t_1 = t_2 = t_3 = 0$ and $t_4 = 2\pi/2^n$, and initiate qubits C_2 and T_2 to $|C_2T_2\rangle = |10\rangle$, we obtain the result in Eq. (3) from above.

Native QFT algorithm with the Diamond gate

Having found a way to apply a controlled R_n gate to all qubits using the diamond gate, we are now ready to consider the problem of performing the quantum Fourier transformation algorithm. This can be done using the circuit seen in Fig. 2. If $|j\rangle$ is a ket in an orthonormal basis, $\{|0\rangle, |1\rangle, \dots, |N-1\rangle\}$, this circuit performs the transformation

$$|j\rangle \mapsto \frac{1}{\sqrt{N}} \sum_{k=0}^{N-1} e^{2\pi i j k / 2^n} |k\rangle, \quad (4)$$

where $N = 2^n$ and n is the number of qubits and $|k\rangle$ denotes the k th basis state [5].

As we wish to perform the QFT algorithm using the diamond gate, we must first figure out how to arrange our qubits. As a starting point we choose to arrange the qubits in two parallel lines as seen in Fig. 3. The

We can therefore place phase gates on all qubits in between the two diamond gates, and thereby obtain controlled phase gates on all qubits. Doing this we obtain the following circuit

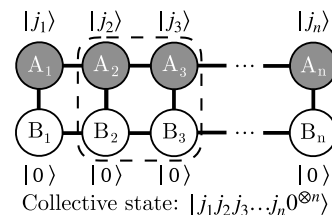


Figure 3. **Qubit structure for implementing QFT.** Two parallel interconnected lines of qubits used in the QFT algorithm. The upper qubits (A) are initialized in the states $|j_1\rangle, \dots, |j_n\rangle$, while the lower qubits are all in the $|0\rangle$ state. Using one pair of A-qubits and one pair of B-qubits a diamond gate can be performed.

upper line contains the target qubits in arbitrary states $|j_1\rangle, \dots, |j_n\rangle$, while the lower line is the auxiliary qubits, all in states $|0\rangle$. Tuning a square of these qubits into resonance makes it possible to perform the diamond gate. This arrangement of qubits has the advantage of the QFT implementation being the most simple, however for a large number of qubits, frequency crowding might lead to an unwanted cross talk in-between qubits. We ignore this problem for now, however, in Fig. 4 we present alternative arrangements of qubits, which makes this problem less severe.

QFT algorithm

Here we present an algorithm for QFT using the topology presented in Fig. 3:

Algorithm 1 Native Gate Assisted QFT on Double-String of Qubits

```

1: Initialize qubits  $A_1, \dots, A_n$  with the states to transform
2: Initialize qubits  $B_1, \dots, B_n$  in state  $|0\rangle^{\otimes n}$ 
3: for  $i = 1$  to  $n$  do                                ▷ For every target state
4:   H on  $A_i$ 
5:   for  $j = i + 1$  to  $n$  do                            ▷ ... for every control state
6:     X on  $B_{j-1}$                                        ▷ Do  $CR_n$  using native gate
7:      $U(t_g)$  on  $(A_j, B_{j-1}, A_{j-1}, B_j)$ 
8:      $R_{j-i+1}$  on  $B_j$ 
9:      $U(t_g)$  on  $(A_j, B_{j-1}, A_{j-1}, B_j)$ 
10:    X on  $B_{j-1}$ 
11:    if  $j \neq n$  then ▷ Swap along chain (except last)
12:       $iSWAP(t_g/2)$  on  $(A_{j-1}, A_j)$ 
13:    end if
14:  end for
15:  for  $j = n - 1$  to  $i + 1$  do ▷ Swap state back home
16:     $iSWAP(3t_g/2)$  on  $(A_{j-1}, A_j)$ 
17:  end for                                            ▷ Done for  $A_i$ 
18: end for
19: Reverse order of A-qubits.

```

It works by iterating through every A-qubit, from A_1 (of state $|j_1\rangle$) to A_n (of state $|j_n\rangle$). First a Hadamard-gate is applied to the A_i 'th qubit. Then a phase gate, controlled by its neighboring A-qubit (A_{i+1}), based upon the diamond gate assisted controlled R_n -gate of Eq. (3). This diamond gate is formed by tuning the diamond of A-qubits (A_i and A_{i+1}), and the associated pair of B-qubits (B_i and B_{i+1}). Then, the pair of A-qubits swaps states through an $iSWAP$ -gate, such that another controlled phase may be applied to the A_{i+1} 'th qubit, which now holds the state of the A_i 'th qubit. This is repeated such that the state originally of the A_i 'th qubit is swapped to the end of the chain. At this point it is swapped back into place, by doing the $iSWAP$'s in reverse.

An important point is, that the initial swaps down the chain are $iSWAP(t_g/2)$, whereas the ones on the way back are $iSWAP(3t_g/2)$. Simply doing $iSWAP(t_g/2)$ twice could leave the pair of states with unwanted phases, but by using $iSWAP(3t_g/2)$ the second time around gets rid of these. Indeed, the trick here is that by swapping the states back through the chain, we ensure that each swapped pair of states will see each other twice. In turn, this will cancel any phase introduced by the initial $iSWAP(t_g/2)$.

This QFT implementation on $O(n)$ input states requires $2n$ qubits. Thus, the number of qubits required grows linearly with the input size. The circuit depth grows as $O(n^2)$ just as the regular QFT algorithm. On top of that, we can easily adapt the method of the approximate QFT, and leave out the smallest of R_n -angles. This would reduce the depth to grow as $O(n \log n)$. But in absolute gate numbers, it does use more than regular QFT, because we have to swap the states along the chain. The absolute

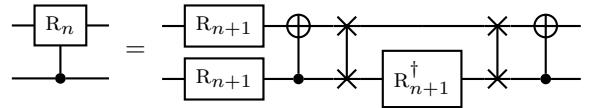
gate counts are thus

- n H gates
- $n(n+1)$ X gates
- $n(n+1)/2$ R_n gates
- $n(n-1)$ $iSWAP$ gates

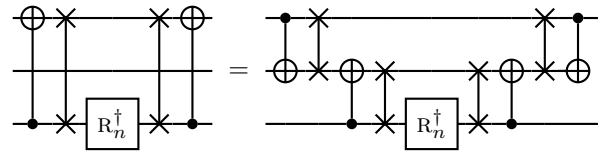
This is without considering the QFT cross-swap of the A qubits at the end. Still the algorithmic part of this procedure does not add asymptotic overhead to the existing QFT algorithm.

Native CNS-gate based QFT algorithm

We wish to implement the QFT algorithm using the diamond version of the CNS gate. Using an identity from Ref. [45] we replace each controlled R_n gate and introduce a pair of swaps to create two CNS gates:

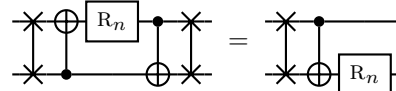


Now, the diamond circuit is only capable of executing CNS gates on opposing qubits, and for the QFT algorithm in Fig. 2 we have to operate between all qubits. However, the CNS gate can also be used to make a pseudo-swap gate for this purpose. Thus, we use pairs of CNS gates to swap the first qubit into place and back again as follows:



This works because of the symmetry of the swapping CNS gate pairs: Between each pair, the qubit at the control will only pick up a phase, and the target one is not transformed at all. Therefore, the effect of the CNS gates will cancel each other, but we can still utilize the swapping functionality in-between.

This algorithm can be run on a chain of diamond circuits, having the CNS gates only work on adjacent qubits. However, this sequence of gates can still be significantly refactored using the identity,



Finally this means that we can write the first part of the QFT algorithm in Fig. 2, which is the QFT of the first qubit, as

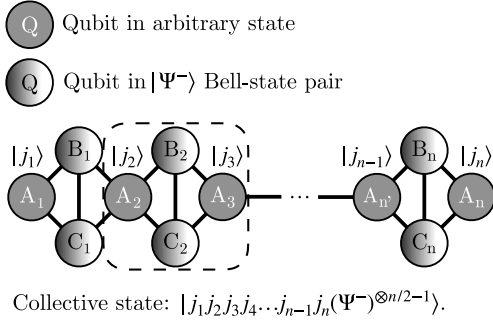
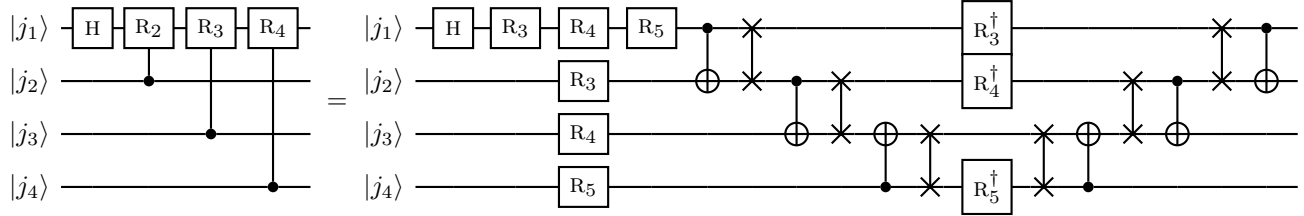


Figure 4. **Alternative qubit structure for implementing QFT.** Chain of concatenated diamond circuits, each sharing a target qubit with its neighbor. This arrangement can be used to execute a CNS gate assisted QFT algorithm.

Now only three similar circuit have to be added, to represent the QFT of all four qubits. In the same way, this method is extensible to even more qubits. In particular, one hardware set-up to execute this algorithm is seen in Fig. 4, which is just a sequence of concatenated diamond circuits, each sharing one qubit with its neighbor. Using this configuration, an additional QFT-qubit requires three extra qubits in the circuit. That is, QFT on n qubits requires $3n + 1$ circuit qubits.

Quantum machine learning with the diamond gate

Another application where the diamond gate could prove itself useful is in hybrid quantum classical algorithms. Examples of this have already been shown in relation to variational quantum eigensolvers [44]. Here we wish to consider the diamond gate in a HQC algorithm for machine learning on near-term quantum processors, namely quantum circuit learning as proposed by Ref. [43]. Besides quantum circuit learning we also wish to consider the problem of classifying data using PQC with the diamond gate as an entangling gate. We do this following the approach taken by Ref. [26].

Quantum circuit learning

Quantum circuit learning is quantum aided machine learning and has been shown to be able to approximate non-linear functions. Quantum circuit learning is done in five steps:

1. Encode input data in some quantum state $|\psi_{\text{in}}(x)\rangle = U_1(x)|0\dots 0\rangle$.
2. Apply parameterized quantum circuit to the input state $|\psi_{\text{out}}(\theta_i, x)\rangle = U_2(\theta_i)|\psi_{\text{in}}(x)\rangle$.
3. Measure expectation values of some chosen observables, B_k . By using some output function F , the output is defined to be $y(x, \theta_i) = F(\{B_k(x, \theta_i)\})$.
4. Minimize the cost function $L(f(x), y(x, \theta_i))$ of the objective function $f(x)$ and output by tuning the parameters θ_i .
5. Evaluate the performance by checking the value of the cost function or a similar evaluation criterion.

We wish to use the diamond gate for approximating a function of one parameters $f: [-1, 1] \rightarrow \mathbb{R}$. We therefore encode quantum state as the density matrix

$$\rho_{\text{in}}(x) = \frac{1}{2^N} \bigotimes_{i=1}^N \left[I + xX_i + \sqrt{1-x^2}Z_i \right], \quad (5)$$

where X_i and Z_i are X and Z rotations on the i th qubit respectively. The density matrix can be generated by single-qubit rotations, $R_Y(\sin^{-1} x)$ and $R_Z(\cos^{-1} x^2)$ on each of the qubits. Our initial state is thus

$$|\psi_{\text{in}}(x)\rangle = \prod_{i=1}^N R_Y^{(i)}(\sin^{-1} x) R_Z^{(i)}(\cos^{-1} x^2) |0\rangle^{\otimes N}. \quad (6)$$

Note that in a practical numerical implementation the continuous variable x must be made discrete. This initialization has the effect that the tensor product state will be a polynomial of order N in x , however, the x^N term is hidden with the observable $X^{\otimes N}$. So in order to access its factor we must use an entangling gate, which in this case shall be the diamond gate, $U(t)$. In order to create a parameterized quantum circuit we apply a general single qubit rotation $U_{\text{rot}}(\theta) = R_Z(\theta_1)R_Y(\theta_2)R_Z(\theta_3)$

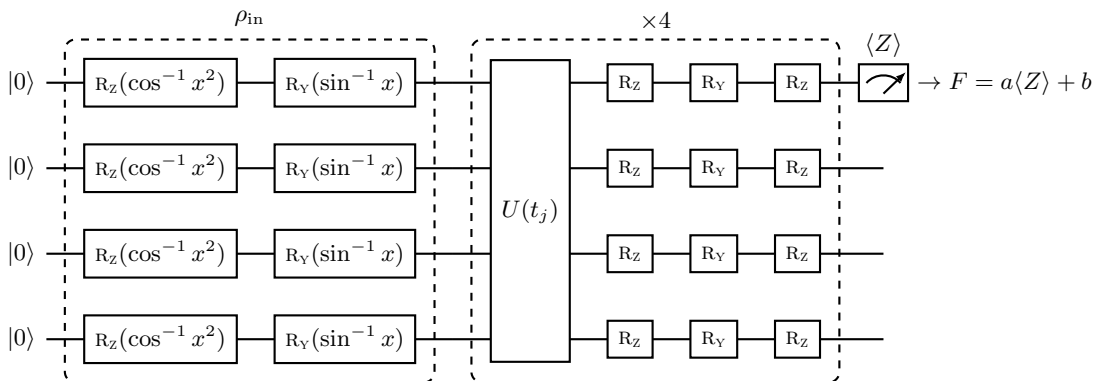


Figure 5. **Circuit diagram of a diamond gate aided circuit learning.** The input data is encoded into the density matrix ρ_{in} using R_z - and R_y -rotations on each qubit, which yield a state similar to Eq. (5). This happens in the left dashed box. The diamond gate, $U(t)$, acts as an entangling gate between the single-qubit rotations. The diamond gate and single-qubit rotations in the right dashed box is repeated four times, with different rotations each time, yielding a four layered parameterized quantum circuit. In the end, the first qubit is measured in the Z basis, and the output scaled and shifted. We optimize the parameters a , b , t_j , as well as the rotation angles of the single-qubit rotations in the right box.

to each of the qubits. The pair of gates, $U(t)$ and $U_{\text{rot}}(\theta)$, are applied several times in layers, each with a different set of parameters. We use four of such layers in our parameterized quantum circuit. At the end, we perform a measurement of the expectation value of Z on the first qubit, which we scale and shift to produce the output function, $F(x, \theta_i) = a\langle Z(x, \theta_i) \rangle + b$. With θ_i being the i th tunable parameter of the circuit, from both $U(t)$ and $U_{\text{rot}}(\theta)$. The resulting gate diagram can be seen in Fig. 5.

We use the quadratic cost function, $L = \|f(x) - F(x, \theta_i)\|^2$ and optimize it using the ADAM optimizer [46]. We test our quantum circuit using the same objective functions as in Ref. [43], namely x^2 , e^x , $\sin x$, and $|x|$, as well as two more difficult functions, $\sin(\pi x) \cos(\pi x/2)$ and $\sin(2\pi x)e^x$. We sample each objective function 100 times as training data. The results of the optimizations can be seen in Fig. 6. As we can see, the parameterized quantum circuit approximates the function reasonably well, even though we are only using four qubits and four layers, where Ref. [43] used six qubit and six layers to obtain the same precision. Reference [43] use a fully connected transverse Ising model as the entangling gate, where we have used the diamond gate to obtain the same results.

Classification of data

Another scheme for quantum machine learning which employs PQC is classification of data points. Once again we will employ a PQC with the diamond gate as the entangling gate, and use it for classification of two-dimensional data points. We follow the approach in Ref. [26] and use the same two-dimensional shapes in order to compare results directly.

The classification of data follows the same algorithm as quantum circuit learning. However, here we use a

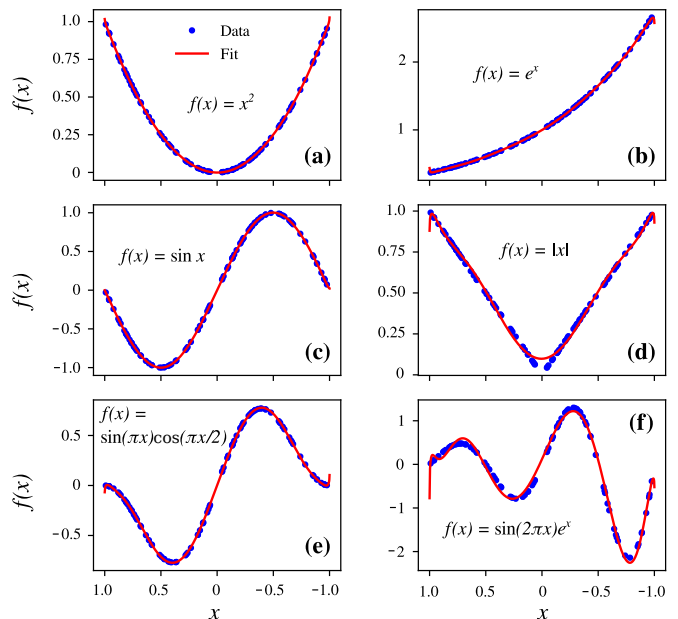


Figure 6. **Diamond assisted quantum circuit learning.** Data (blue points) and fit (red lines) obtained from the diamond assisted quantum circuit learning using the quantum circuit seen in Fig. 5. The fit is given by the function $F(x, \theta_i)$ described in the main text. The parameters, θ_i are tuned to minimize the cost function for all x . The function, $f(x)$, used to sample the blue data points shown are (a) x^2 , (b) e^x , (c) $\sin x$, (d) $|x|$, (e) $\sin(\pi x) \cos(\pi x/2)$, and (f) $\sin(2\pi x)e^x$.

different encoding, following the approach of Ref. [26]. This so-called *minimal expressive embedding* consists of applying single qubit rotations like the encoding used previously. Thus instead of the encoding in Eq. (6) we

use the following one

$$|\psi_{\text{in}}(x)\rangle = \prod_{i=1}^N R_Z^{(i)}(\pi/4) R_Y^{(i)}(\pi/4) R_X^{(i)}(x_i \bmod 2) |0\rangle^{\otimes N}, \quad (7)$$

where we first apply a rotation about the x -axis which depends on x_0 and x_1 in an alternating fashion. We then perform rotations of $\pi/4$ first around the y -axis and then z -axis for all qubits. Following this input encoding, we apply the PQC consisting of the diamond gate, $U(t)$, and a set of general single qubit rotation $U_{\text{rot}}(\theta)$ on each qubit. We apply these last two operations to the state a number of times, one for each layer, that we want in our model. In the end, we measure the expectation value of Z on the first qubit. The result is scaled and shifted and then minimized using a binary cross-entropy function. All in all, we perform the same manipulations of the qubits as in Fig. 5 but with a different encoding, ρ_{in} .

In Fig. 7 we present the nine data sets as well as the classification results for two layers of $U(t)$ and $U_{\text{rot}}(\theta)$. We find the data sets 1b, 2a, and 3a perfectly classified for just a single layer, as well as for more layers. Data set 1a achieves a classification accuracy just above 95% for a single layer, which is the maximal for this data set due to the overlap of the data points. Data sets 2c and 3b also achieve a maximum classification accuracy for a single layer around 73% and 98%, respectively. Data sets 1c and 2b converges at a perfect accuracy for two layers, while the accuracy of the last data set 3c converges for two layers to just above 90%.

As expected we see an almost perfect classification for all data sets except for 2c and 3c, as these are considered the most difficult to classify, due to their complexity. This performance is comparable to the most accurate two-layer-networks used by Ref. [26].

DISCUSSION

We have shown that the native diamond gate [4] may be used beneficially compared to using standard gate sets, which can be difficult to realize on current quantum technology platforms.

First we showed that the diamond gate, together with single qubit gates, can be turned into a controlled-not-swap gate. We then showed how to symmetrically decompose the diamond gate into standard gates in two different ways. Also, by placing a diamond gate on either side of a phase gate we created a controlled phase gate, and argued that this could be used to obtain controlled phase gates on all four qubits. Using this method, we presented an algorithm for the quantum Fourier transform using only single qubit gates alongside the diamond gate.

Finally we applied the diamond gate in quantum machine learning algorithms, and showed that it was useful in a parameterized quantum circuit when used for approximating non-linear functions and classification of two-dimensional data.

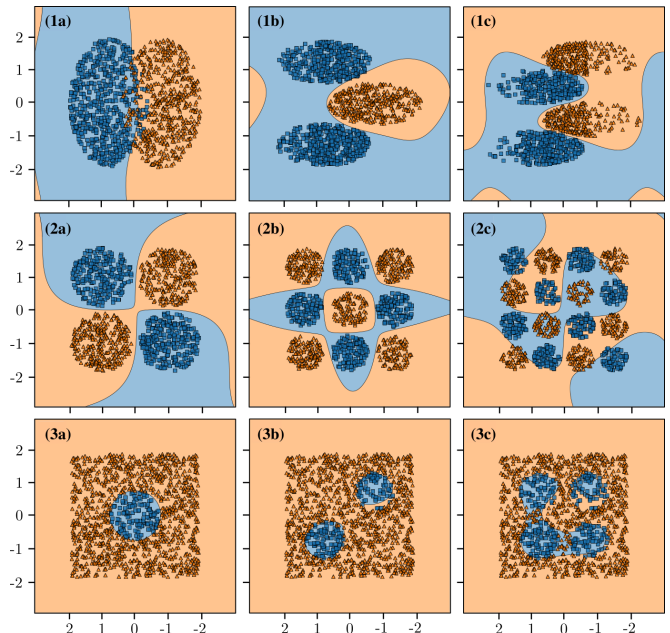


Figure 7. **Diamond assisted quantum circuit classification of two-dimensional data points with two layers.** The squares and triangles (blue and yellow) are the training data replicated from Ref. [26]. The background colors indicate the predicted classification by the quantum circuit.

We believe that these results adumbrate the diamond gate as an important building block in near-future quantum technologies. This, together with the fact that other quantum gates do not occur naturally in many quantum technology schemes, demonstrates that the applications of the diamond gate should be pursued further.

METHODS

The four-qubit Diamond gate

The algorithms presented in this paper are based upon the diamond gate developed in Ref. [4]. Here we present an overview, and details can be found in the original article.

The diamond gate is a highly entangling four-qubit gate which is easily implemented using superconducting circuits. The system consists of two target qubits (T_1 and T_2) and two control qubits (C_1 and C_2). Each pair of control and target qubits are connected with a coupling strength of J . The two control qubits are coupled with a coupling strength of J_C . The system schematics can be seen in Fig. 8(a). A superconducting circuit [49–52] design resulting in the diamond gate could consist of transmon-like qubits [47, 48] coupled by capacitors, as seen in Fig. 8(b).

Using units where $\hbar = 1$, the system is governed by the

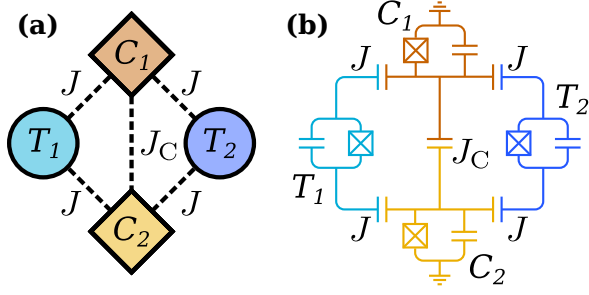


Figure 8. **The Diamond gate** (a) Four-qubit system of two control qubits (C_1 and C_2) and two target qubits (T_1 and T_2), that constitutes the diamond circuit. These couple through their exchange interaction with strengths J and J_C as indicated. (b) An equivalent simple circuit diagram of superconducting transmon qubits [47, 48], which are capacitively coupled with the same strengths J and J_C . Figure, with permission, from Ref. [4].

Hamiltonian

$$H = -\frac{1}{2}(\Omega + \Delta)(\sigma_z^{T_1} + \sigma_z^{T_2}) - \frac{1}{2}\Omega(\sigma_z^{C_1} + \sigma_z^{C_2}) + J_C\sigma_y^{C_1}\sigma_y^{C_2} + J(\sigma_y^{T_1} + \sigma_y^{T_2})(\sigma_y^{C_1} + \sigma_y^{C_2}), \quad (8)$$

where $\sigma_{x,y,z}^j$ are the Pauli operators acting on the j th qubit. The target qubits are in resonance with each other, with frequency $\Omega + \Delta$, while the control qubits are in resonance with frequency Ω .

Assuming $|2\Omega| \gg |J|$ and $|\Delta| \gg |J|, |J_C|$ the time evolution operator of the diamond circuit takes the form

$$U(t) = |00\rangle\langle 00| \otimes U_T^{00}(t) + |11\rangle\langle 11| \otimes U_T^{11}(t) + |\Psi^+\rangle\langle \Psi^+| \otimes U_T^{\Psi^+}(t) + |\Psi^-\rangle\langle \Psi^-| \otimes U_T^{\Psi^-}(t), \quad (9)$$

where the unitary U_T^i acts on the target qubits, while the operators, $|C_1C_2\rangle\langle C_1C_2|$, acts on the control qubits with C_1 and C_2 representing the first and second control qubit respectively. These can be in either of the control states $|00\rangle, |11\rangle, |\Psi^+\rangle, |\Psi^-\rangle$, where $|\Psi^\pm\rangle = (|01\rangle \pm |10\rangle)/\sqrt{2}$ are the Bell states. From Eq. (9) we realize that $U(t)$ is block diagonal in this basis, which we will call the Bell basis. The unitaries of the target qubits are (represented in the computational basis $|T_1T_2\rangle \in \{|00\rangle, |01\rangle, |10\rangle, |11\rangle\}$,

which is used unless noted otherwise)

$$U_T^{00}(t) = \begin{pmatrix} 1 & 0 & 0 & 0 \\ 0 & \frac{1}{2}(e^{-i\zeta t} + 1) & \frac{1}{2}(e^{-i\zeta t} - 1) & 0 \\ 0 & \frac{1}{2}(e^{-i\zeta t} - 1) & \frac{1}{2}(e^{-i\zeta t} + 1) & 0 \\ 0 & 0 & 0 & e^{-i\zeta t} \end{pmatrix}, \quad (10a)$$

$$U_T^{11}(t) = \begin{pmatrix} e^{i\zeta t} & 0 & 0 & 0 \\ 0 & \frac{1}{2}(e^{i\zeta t} + 1) & \frac{1}{2}(e^{i\zeta t} - 1) & 0 \\ 0 & \frac{1}{2}(e^{i\zeta t} - 1) & \frac{1}{2}(e^{i\zeta t} + 1) & 0 \\ 0 & 0 & 0 & 1 \end{pmatrix}, \quad (10b)$$

$$U_T^{\Psi^+}(t) = \begin{pmatrix} e^{i\zeta t} & 0 & 0 & 0 \\ 0 & 1 & 0 & 0 \\ 0 & 0 & 1 & 0 \\ 0 & 0 & 0 & e^{-i\zeta t} \end{pmatrix} e^{-iJ_C t}, \quad (10c)$$

$$U_T^{\Psi^-}(t) = \begin{pmatrix} 1 & 0 & 0 & 0 \\ 0 & 1 & 0 & 0 \\ 0 & 0 & 1 & 0 \\ 0 & 0 & 0 & 1 \end{pmatrix} e^{+iJ_C t}, \quad (10d)$$

where $\zeta = 4J^2/\Delta$. If we consider a gate time of $t_g = \pi/\zeta$ the unitaries of the target qubits can be written in standard gates as

$$U_T^{00}(t_g) = ZZ \cdot CZ \cdot \text{SWAP}, \quad (11a)$$

$$U_T^{11}(t_g) = -CZ \cdot \text{SWAP}, \quad (11b)$$

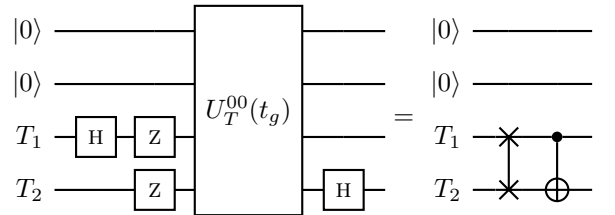
$$U_T^{\Psi^+}(t_g) = -ZZ \cdot e^{-iJ_C t_g}, \quad (11c)$$

$$U_T^{\Psi^-}(t_g) = \Pi \cdot e^{+iJ_C t_g}, \quad (11d)$$

where we have used the notation that $ZZ = Z \otimes Z$ is a Z gate on each of the target qubits. Without external interactions and depending on the choice of coupling strengths, J and J_C , the diamond gate can operate with fidelities above 0.99 and a gate time around 60 ns. Since it only contributes a phase, we set $J_C = 0$ for simplicity.

CNS equivalent circuit

In this section we show that the diamond gate together with single-qubit rotations can produce the useful CNS gate. If we consider the unitary of Eq. (11a) acting on the target qubits, we can construct the following circuit equivalent



from which we can create a combined SWAP and CNOT gate using the $U_T^{00}(t_g)$ unitary. The resulting gate is known as the CNS gate. This gate is in its own right

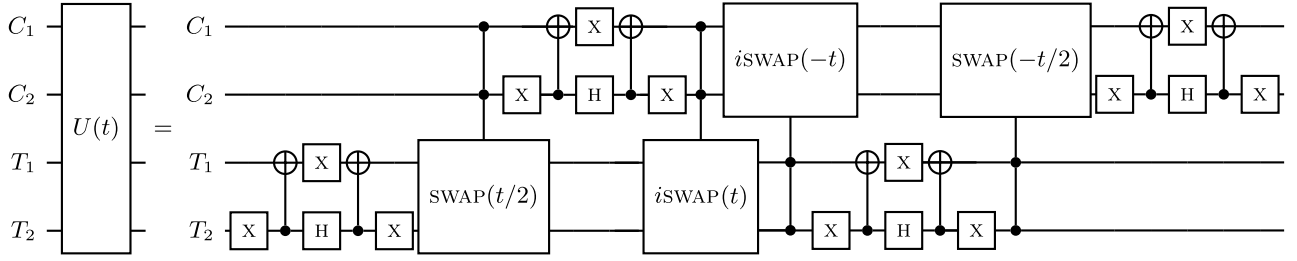


Figure 9. **Standard gate decompositions of the diamond gate with no control coupling, $J_C = 0$, and application time t .** The circuit employs two double-controlled parameterized i SWAP-gates and two double-controlled parameterized SWAP-gates.

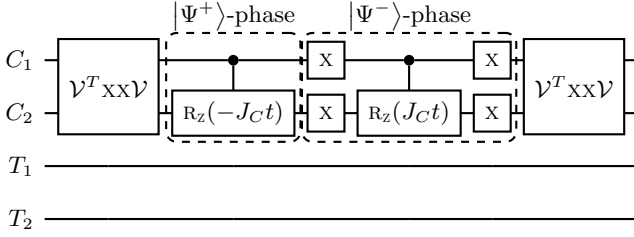


Figure 10. **Circuit diagram adding global phase.** If the control qubits are in the state $|\Psi^\pm\rangle$ the phase $e^{\mp i J_C t}$ is applied. To add this functionality to the diagrams of the diamond gate in the previous section, we will just have to concatenate this to the end of these. This adds the possibility of $J \neq 0$.

-
- [1] F. Arute, K. Arya, R. Babbush, D. Bacon, J. C. Bardin, R. Barends, R. Biswas, S. Boixo, F. G. S. L. Brandao, D. A. Buell, B. Burkett, Y. Chen, Z. Chen, B. Chiaro, R. Collins, W. Courtney, A. Dunsworth, E. Farhi, B. Foxen, A. Fowler, C. Gidney, M. Giustina, R. Graff, K. Guerin, S. Habegger, M. P. Harrigan, M. J. Hartmann, A. Ho, M. Hoffmann, T. Huang, T. S. Humble, S. V. Isakov, E. Jeffrey, Z. Jiang, D. Kafri, K. Kechedzhi, J. Kelly, P. V. Klimov, S. Knysh, A. Korotkov, F. Kostriksa, D. Landhuis, M. Lindmark, E. Lucero, D. Lyakh, S. Mandrà, J. R. McClean, M. McEwen, A. Megrant, X. Mi, K. Michielsen, M. Mohseni, J. Mutus, O. Naaman, M. Neeley, C. Neill, M. Y. Niu, E. Ostby, A. Petukhov, J. C. Platt, C. Quintana, E. G. Rieffel, P. Roushan, N. C. Rubin, D. Sank, K. J. Satzinger, V. Smelyanskiy, K. J. Sung, M. D. Trevithick, A. Vainsencher, B. Villalonga, T. White, Z. J. Yao, P. Yeh, A. Zalcman, H. Neven, and J. M. Martinis, Quantum supremacy using a programmable superconducting processor, *Nature* **574**, 505 (2019).
- [2] S. Bravyi, D. Gosset, R. König, and M. Tomamichel, Quantum advantage with noisy shallow circuits, *Nature Physics* 10.1038/s41567-020-0948-z (2020).
- [3] J. Preskill, Quantum Computing in the NISQ era and beyond, *Quantum* **2**, 79 (2018).
- [4] N. J. S. Loft, M. Kjaergaard, L. B. Kristensen, C. K. Andersen, T. W. Larsen, S. Gustavsson, W. D. Oliver, and N. T. Zinner, Quantum interference device for controlled two-qubit operations, *npj Quantum Information* **6**, 47 (2020).
- [5] M. A. Nielsen and I. L. Chuang, *Quantum Computation and Quantum Information* (Cambridge University Press, 2010).
- [6] G. J. Milburn, Quantum optical fredkin gate, *Phys. Rev. Lett.* **62**, 2124 (1989).
- [7] H. F. Chau and F. Wilczek, Simple realization of the fredkin gate using a series of two-body operators, *Phys. Rev. Lett.* **75**, 748 (1995).
- [8] J. Fiurásek, Linear-optics quantum toffoli and fredkin gates, *Phys. Rev. A* **73**, 062313 (2006).
- [9] J. Fiurásek, Linear optical fredkin gate based on partial-swap gate, *Phys. Rev. A* **78**, 032317 (2008).
- [10] Y.-X. Gong, G.-C. Guo, and T. C. Ralph, Methods for a linear optical quantum fredkin gate, *Phys. Rev. A* **78**, 012305 (2008).
- [11] R. B. Patel, J. Ho, F. Ferreyrol, T. C. Ralph, and G. J. Pryde, A quantum fredkin gate, *Science Advances* **2**, 10.1126/sciadv.1501531 (2016).
- [12] T. Ono, R. Okamoto, M. Tanida, H. F. Hofmann, and S. Takeuchi, Implementation of a quantum controlled-swap gate with photonic circuits, *Scientific Reports* **7**, 45353 EP (2017), article.
- [13] J. A. Smolin and D. P. DiVincenzo, Five two-bit quantum gates are sufficient to implement the quantum fredkin gate, *Phys. Rev. A* **53**, 2855 (1996).

- [14] T. Bækkegaard, L. B. Kristensen, N. J. S. Loft, C. K. Andersen, D. Petrosyan, and N. T. Zinner, Realization of efficient quantum gates with a superconducting qubit-qutrit circuit, *Scientific Reports* **9**, 13389 (2019).
- [15] S. Poletto, J. M. Gambetta, S. T. Merkel, J. A. Smolin, J. M. Chow, A. D. Córcoles, G. A. Keefe, M. B. Rothwell, J. R. Rozen, D. W. Abraham, C. Rigetti, and M. Steffen, Entanglement of two superconducting qubits in a waveguide cavity via monochromatic two-photon excitation, *Phys. Rev. Lett.* **109**, 240505 (2012).
- [16] S. E. Rasmussen, K. S. Christensen, and N. T. Zinner, Controllable two-qubit swapping gate using superconducting circuits, *Phys. Rev. B* **99**, 134508 (2019).
- [17] S. E. Rasmussen, K. Groenland, R. Gerritsma, K. Schoutens, and N. T. Zinner, Single-step implementation of high-fidelity n -bit toffoli gates, *Phys. Rev. A* **101**, 022308 (2020).
- [18] E. Farhi, J. Goldstone, and S. Gutmann, A quantum approximate optimization algorithm (2014), arXiv:1411.4028.
- [19] J. S. Otterbach, R. Manenti, N. Alidoust, A. Bestwick, M. Block, B. Bloom, S. Caldwell, N. Didier, E. S. Fried, S. Hong, P. Karalekas, C. B. Osborn, A. Papageorge, E. C. Peterson, G. Prawiroatmodjo, N. Rubin, C. A. Ryan, D. Scarabelli, M. Scheer, E. A. Sete, P. Sivarajah, R. S. Smith, A. Staley, N. Tezak, W. J. Zeng, A. Hudson, B. R. Johnson, M. Reagor, M. P. da Silva, and C. Rigetti, Unsupervised machine learning on a hybrid quantum computer (2017), arXiv:1712.05771.
- [20] N. Moll, P. Barkoutsos, L. S. Bishop, J. M. Chow, A. Cross, D. J. Egger, S. Filipp, A. Fuhrer, J. M. Gambetta, M. Ganzhorn, A. Kandala, A. Mezzacapo, P. Muller, W. Riess, G. Salis, J. Smolin, I. Tavernelli, and K. Temme, Quantum optimization using variational algorithms on near-term quantum devices, *Quantum Science and Technology* **3**, 030503 (2018).
- [21] J. Romero, J. P. Olson, and A. Aspuru-Guzik, Quantum autoencoders for efficient compression of quantum data, *Quantum Sci. Technol.* **2**, 045001 (2017).
- [22] P. D. Johnson, J. Romero, J. Olson, Y. Cao, and A. Aspuru-Guzik, Qvector: an algorithm for device-tailored quantum error correction (2017), arXiv:1711.02249.
- [23] E. Farhi and H. Neven, Classification with quantum neural networks on near term processors (2018), arXiv:1802.06002.
- [24] V. Havlíček, A. D. Córcoles, K. Temme, A. W. Harrow, A. Kandala, J. M. Chow, and J. M. Gambetta, Supervised learning with quantum-enhanced feature spaces, *Nature* **567**, 209 (2019).
- [25] M. Schuld, A. Bocharov, K. M. Svore, and N. Wiebe, Circuit-centric quantum classifiers, *Phys. Rev. A* **101**, 032308 (2020).
- [26] T. Hubregtsen, J. Pichlmeier, P. Stecher, and K. Bertels, Evaluation of parameterized quantum circuits: on the design, and the relation between classification accuracy, expressibility and entangling capability (2020), arXiv:2003.09887.
- [27] P.-L. Dallaire-Demers and N. Killoran, Quantum generative adversarial networks, *Phys. Rev. A* **98**, 012324 (2018).
- [28] S. Lloyd and C. Weedbrook, Quantum generative adversarial learning, *Phys. Rev. Lett.* **121**, 040502 (2018).
- [29] C. Zoufal, A. Lucchi, and S. Woerner, Quantum generative adversarial networks for learning and loading random distributions, *npj Quantum Information* **5**, 103 (2019).
- [30] D. Zhu, N. M. Linke, M. Benedetti, K. A. Landsman, N. H. Nguyen, C. H. Alderete, A. Perdomo-Ortiz, N. Korda, A. Garfoot, C. Breche, L. Egan, O. Perdomo, and C. Monroe, Training of quantum circuits on a hybrid quantum computer, *Science Advances* **5**, 10.1126/sciadv.aaw9918 (2019).
- [31] A. Peruzzo, J. McClean, P. Shadbolt, M.-H. Yung, X.-Q. Zhou, P. J. Love, A. Aspuru-Guzik, and J. L. O'Brien, A variational eigenvalue solver on a photonic quantum processor, *Nature Communications* **5**, 4213 (2014).
- [32] J. R. McClean, J. Romero, R. Babbush, and A. Aspuru-Guzik, The theory of variational hybrid quantum-classical algorithms, *New Journal of Physics* **18**, 023023 (2016).
- [33] P. J. J. O'Malley, R. Babbush, I. D. Kivlichan, J. Romero, J. R. McClean, R. Barends, J. Kelly, P. Roushan, A. Tranter, N. Ding, B. Campbell, Y. Chen, Z. Chen, B. Chiaro, A. Dunsworth, A. G. Fowler, E. Jeffrey, E. Lucero, A. Megrant, J. Y. Mutus, M. Neeley, C. Neill, C. Quintana, D. Sank, A. Vainsencher, J. Wenner, T. C. White, P. V. Coveney, P. J. Love, H. Neven, A. Aspuru-Guzik, and J. M. Martinis, Scalable quantum simulation of molecular energies, *Phys. Rev. X* **6**, 031007 (2016).
- [34] A. Kandala, A. Mezzacapo, K. Temme, M. Takita, M. Brink, J. M. Chow, and J. M. Gambetta, Hardware-efficient variational quantum eigensolver for small molecules and quantum magnets, *Nature* **549**, 242 (2017).
- [35] Y. Cao, J. Romero, J. P. Olson, M. Degroote, P. D. Johnson, M. Kieferová, I. D. Kivlichan, T. Menke, B. Peropadre, N. P. D. Sawaya, S. Sim, L. Veis, and A. Aspuru-Guzik, Quantum chemistry in the age of quantum computing, *Chemical Reviews* **119**, 10856 (2019).
- [36] P. K. Barkoutsos, J. F. Gonthier, I. Sokolov, N. Moll, G. Salis, A. Fuhrer, M. Ganzhorn, D. J. Egger, M. Troyer, A. Mezzacapo, S. Filipp, and I. Tavernelli, Quantum algorithms for electronic structure calculations: Particle-hole hamiltonian and optimized wave-function expansions, *Phys. Rev. A* **98**, 022322 (2018).
- [37] A. J. McCaskey, Z. P. Parks, J. Jakowski, S. V. Moore, T. D. Morris, T. S. Humble, and R. C. Pooser, Quantum chemistry as a benchmark for near-term quantum computers, *npj Quantum Information* **5**, 99 (2019).
- [38] B. T. Gard, L. Zhu, G. S. Barron, N. J. Mayhall, S. E. Economou, and E. Barnes, Efficient symmetry-preserving state preparation circuits for the variational quantum eigensolver algorithm, *npj Quantum Information* **6**, 10 (2020).
- [39] S. Sim, P. D. Johnson, and A. Aspuru-Guzik, Expressibility and entangling capability of parameterized quantum circuits for hybrid quantum-classical algorithms, *Advanced Quantum Technologies* **2**, 1900070 (2019).
- [40] M. R. Geller, Sampling and scrambling on a chain of superconducting qubits, *Phys. Rev. Applied* **10**, 024052 (2018).
- [41] Y. Du, M.-H. Hsieh, T. Liu, and D. Tao, The expressive power of parameterized quantum circuits (2018), arXiv:1810.11922.
- [42] M. Benedetti, E. Lloyd, S. Sack, and M. Fiorentini, Parameterized quantum circuits as machine learning models, *Quantum Science and Technology* **4**, 043001 (2019).
- [43] K. Mitarai, M. Negoro, M. Kitagawa, and K. Fujii, Quantum circuit learning, *Phys. Rev. A* **98**, 032309 (2018).

- [44] S. E. Rasmussen, N. J. S. Loft, T. Bækkegaard, M. Kues, and N. T. Zinner, Reducing the amount of single-qubit rotations in vqe and related algorithms, *Advanced Quantum Technologies* **3**, 2000063 (2020).
- [45] T. Kim and B.-S. Choi, Efficient decomposition methods for controlled-rnusing a single ancillary qubit, *Scientific Reports* **8**, 5445 (2018).
- [46] D. P. Kingma and J. Ba, Adam: A method for stochastic optimization (2014), arxiv:1412.6980.
- [47] J. Koch, T. M. Yu, J. Gambetta, A. A. Houck, D. I. Schuster, J. Majer, A. Blais, M. H. Devoret, S. M. Girvin, and R. J. Schoelkopf, Charge-insensitive qubit design derived from the cooper pair box, *Phys. Rev. A* **76**, 042319 (2007).
- [48] J. A. Schreier, A. A. Houck, J. Koch, D. I. Schuster, B. R. Johnson, J. M. Chow, J. M. Gambetta, J. Majer, L. Frunzio, M. H. Devoret, S. M. Girvin, and R. J. Schoelkopf, Suppressing charge noise decoherence in superconducting charge qubits, *Phys. Rev. B* **77**, 180502 (2008).
- [49] J. Q. You and F. Nori, Superconducting circuits and quantum information, *Physics Today* **58**, 10.1063/1.2155757 (2005).
- [50] U. Vool and M. Devoret, Introduction to quantum electromagnetic circuits, *International Journal of Circuit Theory and Applications* **45**, 897 (2017), <https://onlinelibrary.wiley.com/doi/pdf/10.1002/cta.2359>.
- [51] P. Krantz, M. Kjaergaard, F. Yan, T. P. Orlando, S. Gustavsson, and W. D. Oliver, A quantum engineer's guide to superconducting qubits, *Applied Physics Reviews* **6**, 021318 (2019).
- [52] S. E. Rasmussen, K. S. Christensen, S. P. Pedersen, L. B. Kristensen, T. Bækkegaard, N. J. S. Loft, and N. T. Zinner, The superconducting circuit companion – an introduction with worked examples (2021), arXiv:2103.01225 [quant-ph].
- [53] N. Schuch and J. Siewert, Natural two-qubit gate for quantum computation using the XY interaction, *Phys. Rev. A* **67**, 032301 (2003).
- [54] T. Tanamoto, K. Maruyama, Y.-x. Liu, X. Hu, and F. Nori, Efficient purification protocols using iSWAP gates in solid-state qubits, *Phys. Rev. A* **78**, 062313 (2008).
- [55] T. Tanamoto, Y.-x. Liu, X. Hu, and F. Nori, Efficient quantum circuits for one-way quantum computing, *Phys. Rev. Lett.* **102**, 100501 (2009).
- [56] A. M. Zagoskin, S. Ashhab, J. R. Johansson, and F. Nori, Quantum two-level systems in josephson junctions as naturally formed qubits, *Phys. Rev. Lett.* **97**, 077001 (2006).
- [57] D. C. McKay, S. Filipp, A. Mezzacapo, E. Magesan, J. M. Chow, and J. M. Gambetta, Universal gate for fixed-frequency qubits via a tunable bus, *Phys. Rev. Applied* **6**, 064007 (2016).
- [58] A. Dewes, F. R. Ong, V. Schmitt, R. Lauro, N. Boulant, P. Bertet, D. Vion, and D. Esteve, Characterization of a two-transmon processor with individual single-shot qubit readout, *Phys. Rev. Lett.* **108**, 057002 (2012).
- [59] Y. Salathé, M. Mondal, M. Oppliger, J. Heinsoo, P. Kurpiers, A. Potočnik, A. Mezzacapo, U. Las Heras, L. Lamata, E. Solano, S. Filipp, and A. Wallraff, Digital quantum simulation of spin models with circuit quantum electrodynamics, *Phys. Rev. X* **5**, 021027 (2015).
- [60] A. Imamoglu, D. D. Awschalom, G. Burkard, D. P. DiVincenzo, D. Loss, M. Sherwin, and A. Small, Quantum information processing using quantum dot spins and cavity qed, *Phys. Rev. Lett.* **83**, 4204 (1999).
- [61] M. Benito, J. R. Petta, and G. Burkard, Optimized cavity-mediated dispersive two-qubit gates between spin qubits, *Phys. Rev. B* **100**, 081412R (2019).
- [62] A. Blais, R.-S. Huang, A. Wallraff, S. M. Girvin, and R. J. Schoelkopf, Cavity quantum electrodynamics for superconducting electrical circuits: An architecture for quantum computation, *Phys. Rev. A* **69**, 062320 (2004).
- [63] H.-F. Wang, X.-Q. Shao, Y.-F. Zhao, S. Zhang, and K.-H. Yeon, Scheme for implementing linear optical quantum iswap gate with conventional photon detectors, *J. Opt. Soc. Am. B* **27**, 27 (2010).
- [64] M. Bartkowiak and A. Miranowicz, Linear-optical implementations of the iswap and controlled not gates based on conventional detectors, *J. Opt. Soc. Am. B* **27**, 2369 (2010).
- [65] C. Godfrin, R. Ballou, E. Bonet, M. Ruben, S. Klyatskaya, W. Wernsdorfer, and F. Balestro, Generalized ramsey interferometry explored with a single nuclear spin qubit, *npj Quantum Information* **4**, 53 (2018).
- [66] S. E. Rasmussen and N. T. Zinner, Simple implementation of high fidelity controlled-iswap gates and quantum circuit exponentiation of non-hermitian gates, *Phys. Rev. Research* **2**, 033097 (2020).
- [67] E. Bahnsen, Native gate exploitation in four-qubit quantum circuit creation (2020), <https://www.bahnsen.dev/masters>.

ACKNOWLEDGMENTS

The authors would like to thank L. B. Kristensen for discussion on different aspects of the work. This work is supported by the Danish Council for Independent Research and the Carlsberg Foundation, and is derived from the Master's thesis of first author E. Bahnsen [67].

AUTHOR CONTRIBUTIONS

E.B., N.J.S.L., and N.T.Z. conceived of and designed the study. E.B. derived the analytical and numerical results, with inputs from N.T.Z., N.J.S.L., and S.E.R. S.E.R. and E.B. wrote the manuscript with input from N.T.Z. and N.J.S.L.

Supplementary Information to Application of the Diamond Gate in Quantum Fourier Transformations and Quantum Machine Learning

E. Bahnsen,¹ S. E. Rasmussen,¹ N. J. S. Loft,¹ and N. T. Zinner^{1,2,*}

¹*Department of Physics and Astronomy, Aarhus University, DK-8000 Aarhus C, Denmark*

²*Aarhus Institute of Advanced Studies, Aarhus University, DK-8000 Aarhus C, Denmark*

(Dated: May 16, 2022)

S1. ALTERNATIVE TOPOLOGIES FOR THE QFT ALGORITHM WITH THE DIAMOND GATE

There are several other ways to combine the diamond gate for the QFT algorithm. Here we discuss two other approaches which might lessen unwanted cross talk and frequency crowding.

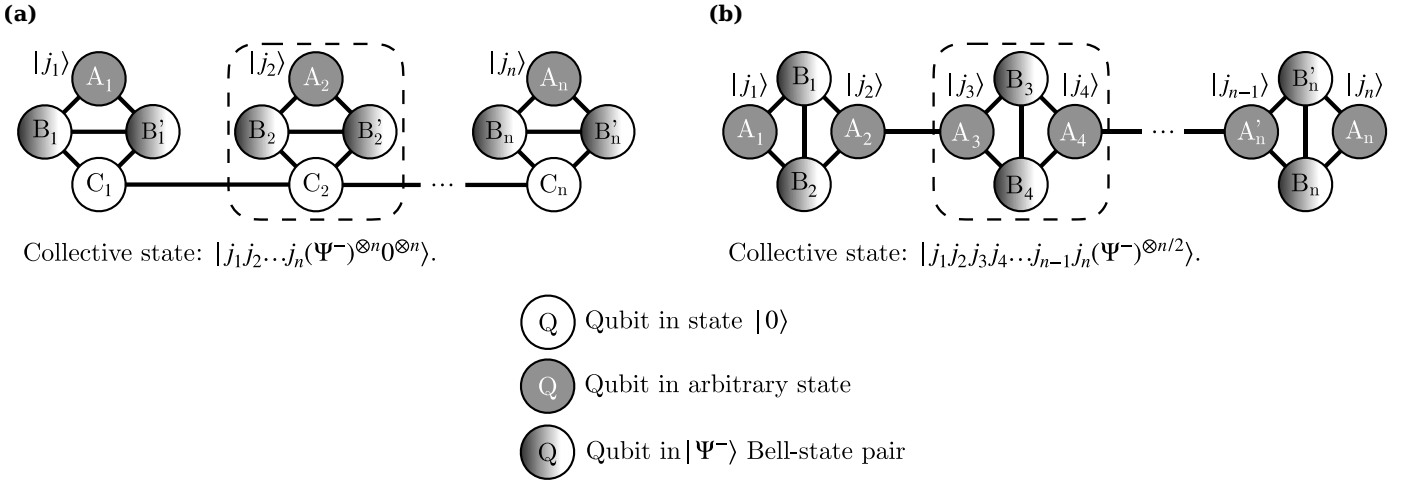


Figure S1. Alternative (to Fig. 7 of the main text) arrangements of multiple diamond circuits interconnected to form a string to execution the diamond gate assisted QFT algorithm. **(a)** The algorithm used for this can be seen in Algorithm S1. With this topology we make use of the idle-state of the diamond, the CNS-gate, and the diamond assisted method of performing a CR_n -gate of Fig. 4 of the main text. **(b)** This configuration is very similar to that of **(a)**, except that we must be more careful when we use the CNS-gate to swap states with. This uses 2 qubits for every input state, as opposed to 4.

An example of such an alternative arrangement of the qubits is seen in Fig. S1(a). Here each diamond is connected via one of the target qubits. The control gates must be prepared in a $|\Psi^-\rangle$ state in order to exploit the idle state of the diamond gate. The non-connected target qubits, A_i , are prepared as the input states, while the connected qubits, C_i s, are prepared in the $|0\rangle$ state. Besides using the idle state of the diamond gate, we also employ the CNS gate. With all the C-qubits in the $|0\rangle$ -state we can use this to swap the states of each A- and C-qubit pair, before this state is send down the line. Each time the state passes a diamond we perform the CR_n as described in the main text. The algorithm used can be seen in Algorithm S1.

* zinner@phys.au.dk

Algorithm S1 Native Gate Assisted QFT on String of Diamonds [Fig. S1(b)]

- 1: Initialize qubits A_1, \dots, A_n with the states to transform $(|j_1\rangle, \dots, |j_n\rangle)$
 - 2: Initialize qubits C_1, \dots, C_n in state $|0\rangle$
 - 3: Initialize qubit pairs $(B_1, B'_1), \dots, (B_n, B'_n)$ in state $|\Psi^-\rangle$
 - 4: **for** $i = 1$ **to** n **do**
 - 5: H on A_i
 - 6: Set qubits B_i and B'_i to $|0\rangle$
 - 7: Swap state of A_i and C_i with diamond CNS-gate
 - 8: Set qubit pair (B_i, B'_i) to $|\Psi^-\rangle$
 - 9: **for** $j = i + 1$ **to** n **do**
 - 10: i SWAP $(t_g/2)$ on (C_{j-1}, C_j)
 - 11: Set qubits B_j and B'_j to $|0\rangle$
 - 12: i SWAP $(t_g/2)$ on (A_j, B_j)
 - 13: R_{j-i+1} on C_j controlled by B_j (using Fig. 4)
 - 14: i SWAP $(3t_g/2)$ on (A_j, B_j)
 - 15: Set qubit pair (B_j, B'_j) to $|\Psi^-\rangle$
 - 16: **end for**
 - 17: Swap state of C_n back to C_i with i SWAP $(3t_g/2)$ or correct for number of i SWAP $(t_g/2)$'s along C-chain (mod 4) and readout state.
 - 18: **end for**
 - 19: Reverse order of C-qubits (these are the output qubits).
-

Another approach to the arrangement of the diamond gates can be seen in Fig. S1(b). In this case only two qubits are used per input state, as opposed to the example in Fig. S1(a) where 4 qubits were used. Like the example in Fig. S1(a) it employs the idle state of the diamond, the CR_n gate and the CNS gate. Using this approach we preserve the input state that is being transformed. That is, the target of the CNS gate acts on the other qubit, and not the one currently being transformed. This is similar to the CNS based pseudo-swap used in the main text.

The algorithm associated with Fig. S1(b) is similar to the one in Algorithm S1. They both use three out of four control states of the diamond gate, $|00\rangle$, $|11\rangle$, and $|\Psi^-\rangle$. Both have the same circuit depth, $O(n^2)$, which can be reduced to $O(n \log n)$ with an approximate QFT approach.

S2. QFT ALGORITHM FOR FOUR QUBITS

Here we present an example of the QFT algorithm for the four qubits in Fig. S2. The final cross-swap is not shown, such that it is clear when each qubit has reached their final state. Dotted lines shows the diamond circuit in use.

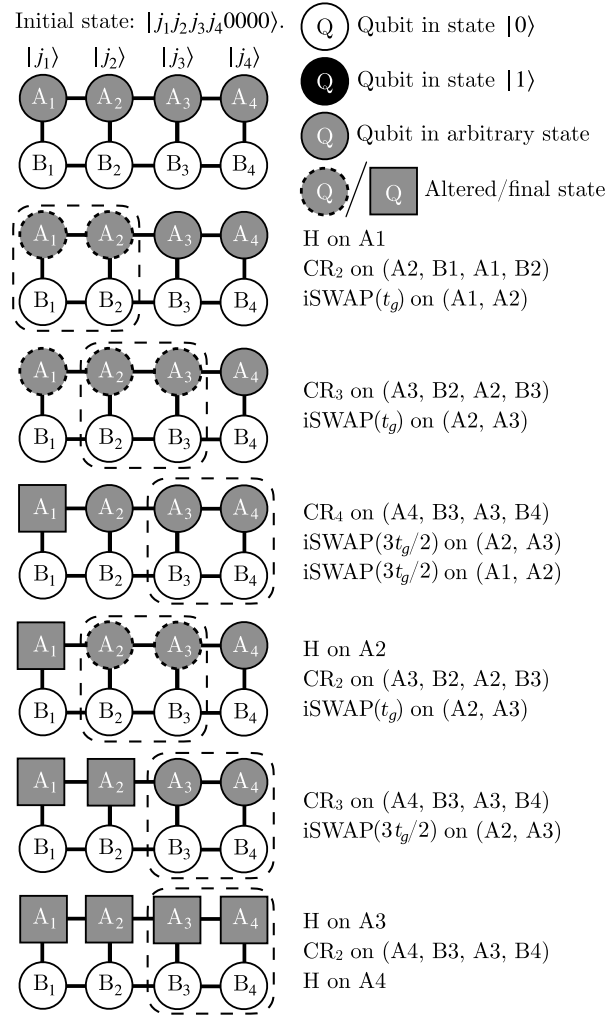


Figure S2. Example of the native gate assisted QFT algorithm for input size $n = 4$. The final cross-swap of A-qubits is not shown, such that the timing of the final states are highlighted. For each step, the dotted lines show the diamond-part of the circuit in use.